IOPscience iopscience.iop.org

Home Search Collections Journals About Contact us My IOPscience

Phenomenological theory of 1–3 type multiferroic composite thin film: thickness effect

This content has been downloaded from IOPscience. Please scroll down to see the full text.

2009 J. Phys. D: Appl. Phys. 42 015309

(http://iopscience.iop.org/0022-3727/42/1/015309)

View the table of contents for this issue, or go to the journal homepage for more

Download details:

IP Address: 113.108.133.53
This content was downloaded on 18/07/2017 at 06:55

Please note that terms and conditions apply.

You may also be interested in:

Critical phase transition temperatures of 1–3 type multiferroic composite thin films
XiaoYan Lu, Biao Wang, Yue Zheng et al.

Polydomain structures in ferroelectric and ferroelastic epitaxial films
Alexander L Roytburd, Jun Ouyang and Andrei Artemev

Coupling interaction in multiferroic BaTiO3–CoFe2O4 nanostructures
Gang Liu, Ce-Wen Nan, Z K Xu et al.

Adjustable ferroelectric properties in paraelectric/ferroelectric/paraelectric trilayers
XiaoYan Lu, Biao Wang, Yue Zheng et al.

Theory of the magnetoelectric effect in multiferroic epitaxial Pb(Zr0.3, Ti0.7)O3/La1.2Sr1.8Mn2O7 heterostructures
ChongGui Zhong and Qing Jiang

Bending response of terfenol-D/BaTiO3 bilayer to external magnetic and electric fields
XiaoYan Lu, Biao Wang, Yue Zheng et al.

Characteristics and controllability of vortices in ferromagnetics, ferroelectrics, and multiferroics
Yue Zheng and W J Chen

Surface tension and size effect in ferroelectric nanotubes
Yue Zheng, C H Woo and Biao Wang

Local polarization dynamics in ferroelectric materials
Sergei V Kalinin, Anna N Morozovska, Long Qing Chen et al.

IOP PUBLISHING JOURNAL OF PHYSICS D: APPLIED PHYSICS

J. Phys. D: Appl. Phys. **42** (2009) 015309 (9pp) doi:10.1088/0022-3727/42/1/015309

Phenomenological theory of 1–3 type multiferroic composite thin film: thickness effect

XiaoYan Lu[1], **Biao Wang**[1,2,4], **Yue Zheng**[1] **and Earle Ryba**[3]

[1] School of Astronautics, Harbin Institute of Technology, Harbin 150001, People's Republic of China
[2] School of Physics and Engineering, Sun Yat-sen University, Guangzhou 510275, People's Republic of China
[3] Department of Materials Science and Engineering, The Pennsylvania State University, University Park, PA, 16802, USA

E-mail: wangbiao@mail.sysu.edu.cn

Received 1 April 2008, in final form 15 October 2008
Published 15 December 2008
Online at stacks.iop.org/JPhysD/42/015309

Abstract

The effect of thickness on the para–ferro-phase transition temperatures, the spontaneous polarization and magnetization and hysteresis loops of 1–3 type multiferroic composite thin films was studied in the framework of Landau phenomenological theory. We took into account the electrostrictive and magnetostrictive effects, misfit strains induced from the interfaces of ferroelectric/ferromagnetic portions and film/substrate. Butterfly loops under external fields were also simulated.

(Some figures in this article are in colour only in the electronic version)

1. Introduction

Multiferroic thin films have attracted much attention because of their potential applications and interesting physical mechanics [1–4]. Experiments using various methods have been conducted to obtain materials with better performance and stronger coupling effect [5, 6]. Usually, single phase materials exhibit only small polarization and magnetization at low temperatures because of the contra-indication between magnetism and ferroelectricity [1]. An alternative route is to combine the piezoelectric materials and magnetostrictive materials. Many samples with different structures [7–9] have been fabricated and large magnetoelectric (ME) effects were achieved. The coupling effects in such composite thin films are believed to be significant with respect to the elastic interaction. Because of the high degree of crystallography orientation, heteroepitaxial composites with spinal ferromagnetic (FM) nanopillars in the ferroelectric (FE) matrix on proper substrates have strong elastic interaction due to the coherency between the phases [10–12].

It is well known that the misfit stress induced from the substrate in a film can strongly affect the properties of FE and FM materials on the nano-scale. By adjusting the stress induced from the substrate, the properties of the film can be controlled. Good connectivity and large contact areas in 1–3 type composite films may result in a significant coupling effect because of the elastic interaction both in the interface of the two portions along the vertical direction and the interface of the film/substrate [13–15]. The stress state in such a structure is very complex because of the existence of dislocations, coupling effects, different thermal expansion coefficients and various defects. Many factors such as the lattice parameters of each part, structure, elastic properties, electrostrictive and magnetostrictive properties can also greatly affect the stress state. In a perfect vertical epitaxial multiferroic composite thin film, the misfit stress induced by the FE/FM and film/substrate interfaces is a key factor to the properties of each component, the stress state and the coupling effect [16, 17]. Stress fields in the composite also have a significant effect on the phase morphologies of the deposited film [18]. It is thus highly desirable to study the stress state in the composites and the ME coupling mechanics to guide the design of such materials.

Many theoretical works have investigated the coupling effect in the nanoscale heterostructures and bulk composites [3, 19]. Green's function technique and phenomenological theory have been developed to describe the coupling effect

---

[4] Author to whom any correspondence should be addressed.

0022-3727/09/015309+09$30.00

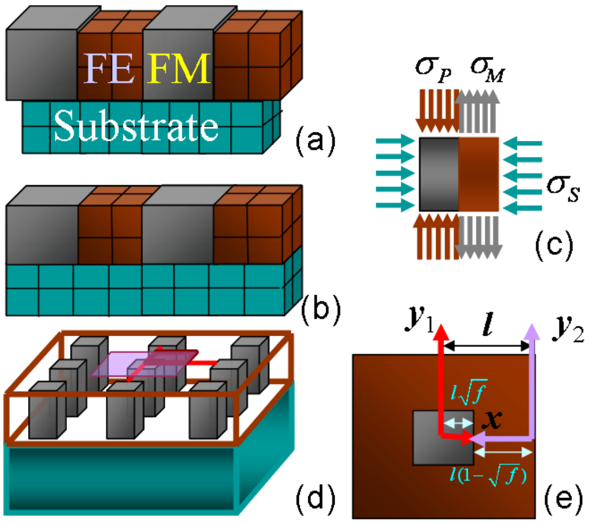

Figure 1. Illustration of calculation model. (*a*) Free standing states of each part; (*b*) state with lattices well matched; (*c*) stress state of each portion of the film, σ_P, σ_M, σ_s are the compressive stress of $BaTiO_3$ on $CoFe_2O_4$, the tensile stress of $CoFe_2O_4$ on $BaTiO_3$ and the average compressive stress of the substrate on the film, respectively; (*d*) heterostructure of the 1–3 type with the FM phase (grey) imbedded in the FE phase (crimson) on a rigid substrate (blue); (*e*) cross section of one element. (Colour online.)

[20, 21]. However, only linear equations with respect to the polarization, magnetization and external fields were used, which does not agree with the experiments of the nonlinear relationship [22].

In this work, we construct a general thermodynamic function to investigate the effect of thickness on the properties of 1–3 type multiferroic thin films based on the Landau mean field theory and Timeshenko's elastic theory. The electrostriction and magnetostriction, misfit induced from the interfaces of FE/FM and film/substrate were considered substantially.

2. Thermodynamic model

A 1–3 type multiferroic thin film with the FM pillars ($CoFe_2O_4$) embedded in the FE matrix ($BaTiO_3$) grown on a rigid substrate $SrTiO_3$ was considered as shown in figure 1. Two local coordinate systems were chosen for the FE and FM phases, respectively. x, y and z are parallel to the [1 0 0], [0 1 0] and [0 0 1] directions of the crystals (figure 1(*e*)). $BaTiO_3$ is cubic in the paraelectric phase and undergoes a cubic-to-tetragonal phase transition when cooled below the critical phase transition temperature [19]. The easy direction of the polarization will be along the direction in which $BaTiO_3$ is under tensile and/or vertical to the direction in which $BaTiO_3$ is under constraint. $CoFe_2O_4$ is unique among ferrites because of its high values of magneto-crystalline anisotropy and magnetostriction [23]. Most important, the lattice parameter is comparable to that of $BaTiO_3$. In the highly strained structure, the nanopillars under constraint will have an easy axis along the z axis [24]. We assumed that the direction of the single domain magnetic component is perpendicular to the interface of the film/substrate.

It is well known that the Curie temperature of FM materials is usually very high and most FM materials are saturated in the room temperature, so the magnitude of magnetization can be assumed as a constant and the direction cosines of the magnetization are often chosen as the variables, such as in the Landau–Lifshitz–Gilbert theory. In this work, we mainly focus on the spontaneous polarization and magnetization in the coupling system other than the domain patterns and evolutions. Ginzburg–Landau theory, which is very useful in the analysis of phase transition and evolution of order parameters, is adopted to describe the fields of spontaneous polarization and magnetization in the FE and FM portions, respectively [25]. The spontaneous polarization P and magnetization M were chosen as the order parameters. We defined P and M as the summations of each small element in the FE and FM portions, respectively. The coupling elastic interaction was dealt with the Timeshenko elastic theory. Since the properties of the material are the same along the x and y axes, the order parameters can be simplified as functions of x and z. The depolarization field may be great in a thin film, but weak in cylinders, especially in the slim cylinders. Ignoring depolarization when a short-circuited electric boundary is used [26], the Helmholtz free energy of the system can be expressed as a sum of the Landau free energies of separated FE and FM portions, the coupling elastic energy and the surface energy [10, 27, 28]:

$$F = F_1^E + F_1^M + F_{\mathrm{surf}} + F_{\mathrm{elas}}, \tag{1}$$

where F_1^E and F_1^M are the Landau type bulk free energies of the FE and FM phases, considering the gradient items because of the inhomogeneous polarization and magnetization in the surface and interface. For FE materials with a first order phase transition and FM materials with a second order phase transition, the bulk free energy density is described by the conventional Landau-type expansions [27]:

$$F_1^E = (1-f)\int_v \left[\frac{A^E}{2}(T-T_{c0}^E)P^2 + \frac{B^E}{4}P^4 + \frac{C^E}{6}P^6 + 2\frac{D_{44}^E}{2}\left(\frac{\partial P}{\partial x}\right)^2 + \frac{D_{11}^E}{2}\left(\frac{\partial P}{\partial z}\right)^2\right]\mathrm{d}v, \tag{2}$$

$$F_1^M = f\int_v \left[\frac{A^M}{2}(T-T_{c0}^M)M^2 + \frac{B^M}{4}M^4 + 2\frac{D_{44}^M}{2}\left(\frac{\partial M}{\partial x}\right)^2 + \frac{D_{11}^M}{2}\left(\frac{\partial M}{\partial z}\right)^2\right]\mathrm{d}v, \tag{3}$$

where A^E, B^E, C^E, D_{44}^E, D_{11}^E and T_{c0}^E are the Landau type bulk free energy expansion coefficients and the Curie temperature for the bulk FE phase. A^M, B^M, D_{44}^M, D_{11}^M and T_{c0}^M are the Landau-type bulk free energy expansion coefficients and the Curie temperature for the bulk FM phase. T is the ambient temperature. f is the volume fraction of the FM phase. v is the volume of the element.

F_{surf} is the surface energy describing the relaxation or restriction energy of the FE and FM parts at the surface and the interface:

$$F_{\mathrm{surf}} = (1-f)\int_{\mathrm{s}} \frac{P^2}{2\delta_{\mathrm{p}z}}\,\mathrm{d}s + f\int_{\mathrm{s}} \frac{M^2}{2\delta_{\mathrm{m}z}}\,\mathrm{d}s + 2\int_{\mathrm{s_i}}\left(\frac{P^2}{2\delta_{\mathrm{p}x}} + \frac{M^2}{2\delta_{\mathrm{m}x}}\right)\mathrm{d}s, \tag{4}$$

where s is the up and bottom surface areas of each element. s_{i} is the interface area between the two phases. $\delta_{\mathrm{p}x}$, $\delta_{\mathrm{p}z}$ and $\delta_{\mathrm{m}x}$, $\delta_{\mathrm{m}z}$ are the extrapolation lengths along the x and z axes for the FE and FM phases, respectively. The extrapolation length describes the difference of the surface and the bulk [29, 30].

F_{elas} is the coupled elastic energy. It can be calculated by finding the elastic strain in each portion separately. The summation of the elastic energies can be written as [16, 31]

$$F_{\mathrm{elas}} = F^{E}_{\mathrm{elas}} + F^{M}_{\mathrm{elas}},$$

$$F^{E}_{\mathrm{elas}} = (1-f)\int_{v} f^{E}_{\mathrm{elas}}\,\mathrm{d}v, \qquad F^{M}_{\mathrm{elas}} = f\int_{v} f^{M}_{\mathrm{elas}}\,\mathrm{d}v, \tag{5}$$

where $f^{E}_{\mathrm{elas}} = \frac{1}{2}C^{E}_{ijkl}e^{\mathrm{p}}_{kl}e^{\mathrm{p}}_{ij} = \frac{1}{2}C^{E}_{ijkl}(\varepsilon^{\mathrm{p}}_{kl} - \varepsilon^{E}_{kl})(\varepsilon^{\mathrm{p}}_{ij} - \varepsilon^{E}_{ij})$, $f^{M}_{\mathrm{elas}} = \frac{1}{2}C^{M}_{ijkl}e^{\mathrm{m}}_{kl}e^{\mathrm{m}}_{ij} = \frac{1}{2}C^{M}_{ijkl}(\varepsilon^{\mathrm{m}}_{kl} - \varepsilon^{M}_{kl})(\varepsilon^{\mathrm{m}}_{ij} - \varepsilon^{M}_{ij})$ are the elastic energy densities in the FE and FM parts, respectively. C^{E}_{ijkl} and C^{M}_{ijkl} are the elastic moduli and e^{p}_{kl}, e^{m}_{kl} are the elastic strain of the FE and FM phases, respectively. $\varepsilon^{\mathrm{p}}_{kl}$, $\varepsilon^{\mathrm{m}}_{kl}$ are the corresponding average total strains, which should be solved through the mechanics balance equations. ε^{E}_{kl} and ε^{M}_{kl} are with respect to the FE and FM spontaneous strains. $\varepsilon^{E}_{ij} = Q^{E}_{ijkl}P_kP_l$ ($P = (P_1, P_2, P_3)$, $k, l = 1, 2, 3$), where Q is the electrostrictive coefficient tensor. $\varepsilon^{M}_{ii} = \frac{3}{2}\lambda_{100}(m_{\mathrm{i}}^2 - \frac{1}{3})$, $\varepsilon^{M}_{ij} = \frac{3}{2}\lambda_{111}m_{\mathrm{i}}m_j(i \neq j, m = M/M_{\mathrm{s}})$ $(m = (m_1, m_2, m_3)$, $i, j = 1, 2, 3)$ [9], where λ_{100}, λ_{111} are the magnetostrictive coefficients of the cubic crystal along the [1 0 0] and [1 1 1] directions. M_{s} is the saturation magnetization of the bulk FM material. In the following, we use Voigt's notation for simplicity. A tensor λ is also introduced to describe the magnetostrictive coefficient, where $\lambda_{11} = \lambda_{22} = \lambda_{33} = 2/3\lambda_{100}$, $\lambda_{12} = \lambda_{13} = \lambda_{23} = 0$ and $\lambda_{44} = \lambda_{55} = \lambda_{66} = \frac{3}{2}\lambda_{111}$.

The electrostrictive strain ε^{E}_{kl} and magnetostrictive strain ε^{M}_{kl} are mediated to each other through the interface of the two portions. The external stress from the substrate due to the lattice misfit between the substrate and the film, the relaxation stress because of the dislocations and the internal stress in the interface of the two portions induced by the lattice mismatch of the FE and FM materials are also coupled together. All the stresses should keep a mechanics balance. By solving the mechanics and displacement balance equations, the elastic strain and stress can be found, then we can derive the elastic energy.

First, we found out the in-plane total strain. Considering a rigid substrate and ignoring the distortion in the film, if the lattices of the substrate and the film are the same, the average total in-plane strain induced by the substrate can be written as a function of the volume fraction

$$\varepsilon^{\mathrm{p}}_{11} = \varepsilon^{\mathrm{p}}_{22} = \varepsilon^{\mathrm{m}}_{11} = \varepsilon^{\mathrm{m}}_{22} = \varepsilon^{0}_{11} = \left(\frac{\sqrt{f}}{\tilde{a}_{\mathrm{m}}} + \frac{1-\sqrt{f}}{a_{\mathrm{p}}}\right)a^{\mathrm{eff}}_{\mathrm{s}} - 1, \tag{6}$$

where a_{p} and $a_{\mathrm{m}} = 2\tilde{a}_{\mathrm{m}}$ are the lattice parameters of the FE and FM materials, respectively. Misfit dislocation formation will relax the strain due to lattice mismatch between each phase. The number of the dislocation varies with the thickness of the film. We induced such a thickness-dependent relaxation by using an effective substrate lattice parameter [32]

$$a^{\mathrm{eff}}_{\mathrm{s}} = \frac{a_{\mathrm{s}}}{\rho a_{\mathrm{s}} + 1}, \qquad \rho = \frac{\varepsilon^{0'}_{11}}{a_0}\left(1 - \frac{h_\rho}{h}\right), \tag{7}$$

where a_{s} is the lattice parameter of the substrate and h is the thickness of the film. ρ is the equilibrium linear dislocation density at the deposition temperature,

$$\varepsilon^{0'}_{11} = 1 - \frac{1}{a_{\mathrm{s}}} \times \frac{\tilde{a}_{\mathrm{m}}a_{\mathrm{p}}}{\sqrt{f}a_{\mathrm{p}} + (1-\sqrt{f})\tilde{a}_{\mathrm{m}}}$$

and $a_0 = \sqrt{f}\tilde{a}_{\mathrm{m}} + (1-\sqrt{f})a_{\mathrm{p}}$ are the average misfit strain and in-plane lattice parameter of the film at the growth temperature, respectively. $h_\rho = \sqrt{f}h^{\mathrm{m}}_\rho + (1-\sqrt{f})h^{\mathrm{p}}_\rho$ is the average critical thickness. h^{p}_ρ and h^{m}_ρ are critical thicknesses of the FE and FM films, respectively, below which dislocation is not feasible.

Second, we derived the vertical total strain $\varepsilon^{\mathrm{p}}_{33}$ in the FE portion and $\varepsilon^{\mathrm{m}}_{33}$ in the FM portion. They can be solved from the mechanical equilibrium equation for the whole sample body subjected to the surface free condition $(1-f)\sigma^{E}_{33} + f\sigma^{M}_{33} = 0$ and the displacement consistent condition in the interface. Both theories and experiments have shown that the strain distribution along the x axis is not uniform because of the large mismatch in the FE/FM interface [31]. We use an average strain to approximate such a phenomenon. Because of the small diameter of the pillars and the high quality of the epitaxial heterostructure, we ignored the dislocations in the interface of the FE and FM parts. The displacement consistent condition in the interface can be written as

$$a_{\mathrm{p}}\frac{\varepsilon^{\mathrm{p}}_{33}}{1-f} - a_{\mathrm{m}}\frac{\varepsilon^{\mathrm{m}}_{33}}{f} = \Delta.$$

$\Delta = \tilde{a}_{\mathrm{m}} - a_{\mathrm{p}}$ is the lattice misfit of the two phases in the vertical direction. The average total stress in the FE part $\varepsilon^{\mathrm{p}}_{33}$ and in the FM part $\varepsilon^{\mathrm{m}}_{33}$ can be written as

$$\begin{aligned} \varepsilon^{\mathrm{p}}_{33} &= \frac{-1}{C_{11E}}(2C^{0}_{12}\varepsilon^{0}_{11} - q^{E}_{11}P^2 + f_{\mathrm{m}}), \\ \varepsilon^{\mathrm{m}}_{33} &= \frac{-1}{C_{11M}}(2C^{0}_{12}\varepsilon^{0}_{11} - q^{M}_{11}M^2/M_{\mathrm{s}}^2 + f_{\mathrm{p}}), \end{aligned} \tag{8}$$

where $C^{0}_{12} = (1-f)C^{E}_{12} + fC^{M}_{12}$, $C_{11E} = (1-f)C^{E}_{11} + (f^2/(1-f))C^{M}_{11}\frac{a_{\mathrm{p}}}{a_{\mathrm{m}}}$ and $C_{11M} = fC^{M}_{11} + ((1-f)^2/f)C^{E}_{11}\frac{a_{\mathrm{m}}}{a_{\mathrm{p}}}$ are the average elastic moduli considering the elastic coupling interaction. $q^{E}_{11} = (1-f)(2C^{E}_{12}Q_{12} + C^{E}_{11}Q_{11})$, $q^{M}_{11} = f(2C^{M}_{12}\lambda_{12} + C^{M}_{11}\lambda_{11})$, $f_{\mathrm{m}} = -f[(2C^{M}_{12}\lambda_{12} + C^{M}_{11}\lambda_{11})(m^2 - 1/3) + fC^{M}_{11}(\Delta/a_{\mathrm{m}})]$, $f_{\mathrm{p}} = -(1-f)[(2C^{E}_{12}Q_{12} + C^{E}_{11}Q_{11})P^2 - (1-f)C^{E}_{11}(\Delta/a_{\mathrm{p}})]$. f_{m} is the item of the magnetization contribution to the polarization and f_{p} is the reverse one. Substituting the above results back into equation (5), the elastic energy density functions can be obtained.

The temporal evolution of the polarization fields can be derived by approaching the Helmholtz free energy at a rate proportional to the consequent Helmholtz free energy change [33]:

$$
\begin{aligned}
\frac{\partial P(x,z,t)}{\partial t} &= -L^E \frac{\delta F}{\delta P(x,z,t)} \\
&= -L^E(1-f)\Bigg[A^E(T-T^E_{\rm c0})P + B^E P^3 \qquad (9) \\
&\quad + C^E P^5 - 2D^E_{44}\frac{\partial^2 P}{\partial x^2} - D^E_{11}\frac{\partial^2 P}{\partial z^2} + \frac{\partial f^E_{\rm elas}}{\partial P}\Bigg], \\
\frac{\partial M(x,z,t)}{\partial t} &= -L^M \frac{\delta F}{\delta M(x,z,t)} \\
&= -L^M f\Bigg[A^M(T-T^M_{\rm c0})M + B^M M^3 \qquad (10) \\
&\quad - 2D^M_{44}\frac{\partial^2 M}{\partial x^2} - D^M_{11}\frac{\partial^2 M}{\partial z^2} + \frac{\partial f^M_{\rm elas}}{\partial M}\Bigg],
\end{aligned}
$$

where L^E and L^M are the kinetic coefficients concerning the domain wall mobility. $A^M = T^M_{\rm c0}/(2\chi)$ and $B^M = 1/(2\chi)$.

Variations of the expression for the elastic energy (equation (5)) with respect to the polarization and the magnetization order parameters are

$$
\begin{aligned}
\partial f^E_{\rm elas}/\partial P &= -2P[(q_{\rm c11} - 2q_{\rm c33}C^0_{12}/C_{11E})\varepsilon^0_{11} \\
&\quad - f_{\rm m}q_{\rm c33}/C_{11E} + 2P^3(q_{\rm c}q - q_{\rm c33}q^E_{11}/C_{11E})], \qquad (11)
\end{aligned}
$$

$$
\begin{aligned}
\partial f^M_{\rm elas}/\partial M &= -2M\lambda_{11}/M_{\rm s}^2\Bigg[2(C^M_{12} - C^M_{11}C^0_{12}/C_{11M})\varepsilon^0_{11} \\
&\quad + \frac{1}{3}C^M_{11}(\lambda_{11} - q^M_{11}/C_{11M}) - f_{\rm p}C^M_{11}/C_{11M}\Bigg] \\
&\quad + 2M^3C^M_{11}\lambda_{11}/M_{\rm s}^4(\lambda_{11} - q^M_{11}/C_{11M}), \qquad (12)
\end{aligned}
$$

where $q_{\rm c11} = 2Q_{12}(C^E_{11} + C^E_{12}) + 2Q_{11}C^E_{12}$, $q_{\rm c33} = 2Q_{12}C^E_{12} + Q_{11}C^E_{11}$, $q_{\rm c}q = Q_{12}[2Q_{12}(C^E_{11} + C^E_{12}) + 2Q_{11}C^E_{12}] + Q_{11}(2Q_{12}C^E_{12} + Q_{11}C^E_{11})$.

Substituting these results into equations (8) and (9), the dynamic equations of the polarization and magnetization considering the elastic interaction are

$$
\begin{aligned}
\frac{\partial P(x,z,t)}{\partial t} &= -L^E \frac{\delta F}{\delta P(x,z,t)} \\
&= -L^E(1-f)\Bigg[A^{E^*}P + B^{E^*}P^3 + C^E P^5 \qquad (13) \\
&\quad - 2D^E_{44}\frac{\partial^2 P}{\partial x^2} - D^E_{11}\frac{\partial^2 P}{\partial z^2}\Bigg], \\
\frac{\partial M(x,z,t)}{\partial t} &= -L^M \frac{\delta F}{\delta M(x,z,t)} \\
&= -L^M f\Bigg[A^{M^*}M + B^{M^*}M^3 \qquad (14) \\
&\quad - 2D^M_{44}\frac{\partial^2 M}{\partial x^2} - D^M_{11}\frac{\partial^2 M}{\partial z^2}\Bigg],
\end{aligned}
$$

where

$$
\begin{aligned}
A^{E^*} &= A^E(T - T^E_{\rm c0}) - 2\Bigg[\left(q_{\rm c11} - 2\frac{q_{\rm c33}}{C_{11E}}C^0_{12}\right)\varepsilon^0_{11} \\
&\quad - \frac{q_{\rm c33}}{C_{11E}}f_{\rm m}\Bigg], \\
B^{E^*} &= B^E + 2\left(q_{\rm c}q - \frac{q_{\rm c33}}{C_{11E}}q^E_{11}\right), \\
A^{M^*} &= A^M(T - T^M_{\rm c0}) - 2\lambda_{11}/M_{\rm s}^2\Bigg[2\left(C^M_{12} - 2\frac{C^M_{11}}{C_{11M}}C^0_{12}\right)\varepsilon^0_{11} \\
&\quad + \frac{1}{3}C^M_{11}\left(\lambda_{11} - \frac{q^M_{11}}{C_{11M}}\right) - \frac{C^M_{11}}{C_{11M}}f_{\rm p}\Bigg], \\
B^{M^*} &= B^M + 2/M_{\rm s}^2\lambda_{11}C^M_{11}\left(\lambda_{11} - \frac{C^M_{11}}{C_{11E}}q^M_{11}\right).
\end{aligned}
$$

The surface items yield the boundary conditions as

$$
\begin{aligned}
&\frac{\partial P}{\partial z} = \mp\frac{P}{\delta_{\rm pz}}\left(z = \pm\frac{h}{2}\right); \frac{\partial P}{\partial x} = -\frac{P}{\delta_{\rm px}}(x = l_{\rm p}), \\
&\frac{\partial P}{\partial n} = 0, \quad (x = 0), \qquad (15) \\
&\frac{\partial M}{\partial z} = \mp\frac{M}{\delta_{\rm mz}}\left(z = \pm\frac{h}{2}\right); \frac{\partial M}{\partial x} = -\frac{M}{\delta_{\rm px}}(x = l_{\rm m}), \\
&\frac{\partial M}{\partial n} = 0, \quad (x = 0),
\end{aligned}
$$

where $l_{\rm p} = (1 - \sqrt{f})l$ and $l_{\rm m} = \sqrt{f}l$ by considering element length l of the sample as shown in figure 1(*d*). h is the thickness of the film.

2.1. *Critical conditions and the phase transition temperatures*

According to the linear stability analysis, the phase transition temperature is relative to the linear item of the evolution equation. The thickness effect on the phase transition temperature can be studied to probe other material properties according to some phenomenological relations. Using the linear analysis theory [34], we apply infinitesimal perturbations $\Delta_{\rm p}$ and $\Delta_{\rm m}$ to the trivial stationary solutions $P_0 = 0$ and $M_0 = 0$. Neglecting the small higher order terms, equations (9) and (10) become

$$
\frac{\partial \Delta_{\rm p}}{\partial t} = -L^E(1-f)\left(A^{E^*}\Delta_{\rm p} - D^E_{11}\frac{\partial^2\Delta_{\rm p}}{\partial z^2} - 2D^E_{44}\frac{\partial^2\Delta_{\rm p}}{\partial x^2}\right), \qquad (16)
$$

$$
\frac{\partial \Delta_{\rm m}}{\partial t} = -L^M f\left(A^{M^*}\Delta_{\rm m} - D^M_{11}\frac{\partial^2\Delta_{\rm m}}{\partial z^2} - 2D^M_{44}\frac{\partial^2\Delta_{\rm m}}{\partial x^2}\right). \qquad (17)
$$

By separating variables and applying the boundary conditions, we can find the para–ferro temperatures [33]

$$
\begin{aligned}
T^E_{\rm c} &= T^E_{\rm c0} - \frac{1}{A^E}(D^E_{11}k^2_{\rm pz} + 2D^E_{44}k^2_{\rm px}) + \frac{2}{A^E}[(q_{\rm c11} \\
&\quad - 2q_{\rm c33}C^0_{12}/C_{11E})\varepsilon^0_{11} - f_{\rm m}q_{\rm c33}/C_{11E}], \qquad (18)
\end{aligned}
$$

$$T_{\mathrm{c}}^M = T_{\mathrm{c0}}^M - \frac{1}{A^M}(D_{11}^M k_{\mathrm{m}z}^2 + 2D_{44}^M k_{\mathrm{m}x}^2) + \frac{2}{A^M M_{\mathrm{s}}^2}\lambda_{11}\bigg[(C_{12}^M - C_{11}^M C_{12}^0/C_{11M})2\varepsilon_{11}^0 - C_{11}^M f_{\mathrm{p}}/C_{11M} + \frac{1}{3}C_{11}^M(\lambda_{11} - q_{11}^M/C_{11M})\bigg]. \quad (19)$$

The smallest values of $k_{\mathrm{p}z}$, $k_{\mathrm{p}x}$, $k_{\mathrm{m}z}$, $k_{\mathrm{m}x}$ can be found from the boundary conditions. Substituting the results into equations (18) and (19), we can obtain the critical temperatures for the phase transitions.

2.2. Spontaneous polarization and magnetization

For applications of multiferroic memories and some multifunctional devises, large spontaneous polarization and magnetization are expected. In these 1–3 type heterostructures, the spontaneous polarization and magnetization are coupled together though the interface of the two portions. The evolution of the spontaneous polarization and magnetization can be obtained by numerically solving the time-dependent Ginzberg–Landau equations (12) and (13) subjected to the boundary conditions. We use the finite-difference method for the time and spatial integration. In each time step, the average polarization and magnetization are calculated to substitute into the stress formulae for the next time step integration. The spontaneous polarization and magnetization can be found in the stable state of the coupling equations at zero external fields.

2.3. Stress field

As shown in equation (8), the average total stress in the FE part $\varepsilon_{33}^{\mathrm{p}}$ and in the FM part $\varepsilon_{33}^{\mathrm{m}}$ are coupled together though the items f_{m} and f_{p}. Both $\varepsilon_{33}^{\mathrm{p}}$ and $\varepsilon_{33}^{\mathrm{m}}$ are functions of spontaneous polarization P and magnetization M. To probe the final stress fields in each composite, we should first derive the stable polarization and magnetization in each composite. The stable polarization and magnetization fields, which is spatially inhomogeneous, can be solved from the dynamic evolution equations by using the numerical method. The average P and M can be derived though $\langle P\rangle = 1/v_{\mathrm{p}}\int_{v_{\mathrm{p}}} P\,\mathrm{d}v$, $\langle M\rangle = 1/v_{\mathrm{m}}\int_{v_{\mathrm{m}}} M\,\mathrm{d}v$, v_{p} and v_{m} are the volumes of the FE and FM portions in the calculated element. Substituting the average P and M back into equations (7), the average vertical total strains in each portion can be found.

2.4. Hysteresis loops

Hysteresis loops, as an important profile of the FE and FM materials, have not been studied for multiferroic composites in a theoretical approach. We use the Landau–Khalatnikor theory to simulate the hysteresis loops [35]. We note that it is just a mathematic approach other than the real physical process, in which the coupled states in FE and FM portion should be real at each time.

We assume that the lattices of each component are matched well, and the FE and FM components have the same thickness (as shown in figure 1(*b*)). Each part can be considered as the stacking of thin layers with a finite thickness $\Delta z = (h/N)$ along the z direction. h is the thickness of the film and N is the number of this layer stack. If the origin is located at the bottom of the film surface, then an arbitrary layer located at a position z can be identified by the index i, $z = i\Delta z$. The polarization, magnetization and the vertical external fields (with the same direction with the polarization) within this layer are denoted by $P^{(i)}$, $M^{(i)}$ and $E^{(i)}$, $H^{(i)}$ in the layer i. The total free energy of the system F_{T} then can be written as the summation of each layer's energy [16]:

$$F_{\mathrm{T}} = \sum_{i=1}^{N} F_{1E}^{(i)} + F_{1M}^{(i)} + F_E^{(i)} + F_H^{(i)} + F_{\mathrm{ela}}^{(i)} + F_{\mathrm{surf}}^{(i)}, \quad (20)$$

where $F_{1E}^{(i)}$ and $F_{1M}^{(i)}$ are the Landau type bulk free energies of the FE phase and FM phases in the i layer, respectively; $F_E^{(i)} = -E^{(i)}P^{(i)}$ and $F_H^{(i)} = -H^{(i)}M^{(i)}$ are the energy induced by the external electric and magnetic fields, respectively; $F_{\mathrm{ela}}^{(i)}$ is the elastic energy; $F_{\mathrm{surf}}^{(i)}$ is the surface energy describing the relaxation of the surface lattices and the relaxation or restriction of the interfacial lattice. $F_{1E}^{(i)}$, $F_{1M}^{(i)}$ and $F_{\mathrm{surf}}^{(i)}$ can be expressed as follows:

$$F_{1E}^{(i)} = (1-f)\int_v \bigg[\frac{A^{E^*}}{2}(T - T_{\mathrm{c0}}^E)(P^{(i)})^2 + \frac{B^{E^*}}{4}(P^{(i)})^4 + \frac{C^E}{6}(P^{(i)})^6 + \kappa_E^{(i)}(P^{(i)} - P^{(i-1)})^2\bigg]\,\mathrm{d}v, \quad (21)$$

$$F_{1M}^{(i)} = f\int_v \bigg[\frac{A^{M^*}}{2}(T - T_{\mathrm{c0}}^M)(M^{(i)})^2 + \frac{B^{M^*}}{4}(M^{(i)})^4 + \kappa_M^{(i)}(M^{(i)} - M^{(i-1)})^2\bigg]\,\mathrm{d}v, \quad (22)$$

$$F_{\mathrm{surf}}^{(i)} = (1-f)\int_{\mathrm{s}} \frac{(P^{(i)})^2}{2\delta_{\mathrm{p}z}}\,\mathrm{d}s + f\int_{\mathrm{s}} \frac{(M^{(i)})^2}{2\delta_{\mathrm{m}z}}\,\mathrm{d}s + \int_{\mathrm{s}_i}\left(\frac{(P^{(i)})^2}{2\delta_{\mathrm{p}x}} + \frac{(M^{(i)})^2}{2\delta_{\mathrm{m}x}}\right)\mathrm{d}s. \quad (23)$$

$\kappa_E^{(i)}$ and $\kappa_M^{(i)}$ are the coupling coefficients between the nearest neighbouring layers.

The dynamic equations of the polarization and magnetization considering the elastic interaction are

$$\frac{\partial P^{(i)}}{\partial t} = -L^E\frac{\delta F^{(i)}}{\delta P^{(i)}} = -L^E(1-f)[A^{E^*}P^{(i)} + B^{E^*}(P^{(i)})^3 + C^E(P^{(i)})^5 - E^{(i)} - \kappa_E^{(i)}(P^{(i+1)} + P^{(i-1)} - 2P^{(i)})], \quad (24)$$

$$\frac{\partial M^{(i)}}{\partial t} = -L^M\frac{\delta F^{(i)}}{\delta M^{(i)}} = -L^M f[A^{M^*}M^{(i)} + B^{M^*}(M^{(i)})^3 - H^{(i)} - \kappa_M^{(i)}(M^{(i+1)} + M^{(i-1)} - 2M^{(i)})]. \quad (25)$$

The surface items yielded the boundary conditions as

$$\frac{\partial P^{(i)}}{\partial z} = \mp\frac{P^{(i)}}{\delta_{\mathrm{p}z}}, \quad \frac{\partial M^{(i)}}{\partial z} = \mp\frac{M^{(i)}}{\delta_{\mathrm{m}z}} \qquad \left(z = \pm\frac{h}{2}\right). \quad (26)$$

Table 1. Parameters of the FE and FM phases.

$BaTiO_3$	$CoFe_2O_4$
$C^E_{11} = C^E_{22} = C^E_{33} = 1.76 \times 10^{11}\,\mathrm{N\,m^{-2}}$	$C^M_{11} = C^M_{22} = C^M_{33} = 2.86 \times 10^{11}\,\mathrm{N\,m^{-2}}$
$C^E_{12} = C^E_{13} = C^E_{23} = 0.846 \times 10^{11}\,\mathrm{N\,m^{-2}}$	$C^M_{12} = C^M_{13} = C^M_{23} = 1.73 \times 10^{11}\,\mathrm{N\,m^{-2}}$
$Q_{11} = Q_{22} = Q_{33} = 0.11\,\mathrm{m^4\,C^{-2}}$,	$\lambda_{100} = -590 \times 10^{-6}$
$Q_{12} = Q_{13} = Q_{23} = -0.043\,\mathrm{m^4\,C^{-2}}$	$\lambda_{111} = 120 \times 10^{-6}$
$a_p = 0.399\,94\,\mathrm{nm}$ ($a_s = 0.3905\,\mathrm{nm}$),	$a_m = 0.838\,\mathrm{nm}$, $\tilde{a}_m = 0.419\,\mathrm{nm}$,
$h^p_\rho = 25\,\mathrm{nm}$	$h^m_\rho = 25\,\mathrm{nm}$
$A^E = 6.6 \times 10^5\,\mathrm{m\,F^{-1}\,K^{-1}}$	$M_s = 300 \times 10^3\,\mathrm{A\,m^{-1}}$
$B^E = 14.4 \times 10^6 \times (T - 448.15)\,\mathrm{m^5\,C^{-2}F^{-1}}$	$\chi = 0.6 \times 10^4\,\mathrm{A\,m^{-1}\,T^{-1}}$, $T^M_{c0} = 793\,\mathrm{K}$
$C^E = 3.96 \times 10^{10}\,\mathrm{m^9\,C^{-4}\,F^{-1}}$	$D^M_{11} = 7.2 \times 10^{-17}$, $D^M_{44} = 3.6 \times 10^{-17}\,\mathrm{J\,m\,A^{-2}}$
$D^E_{11} = 2.7 \times 10^{-9}$, $D^E_{44} = 0.45 \times 10^{-9}\,\mathrm{m^3\,F^{-1}}$	$\delta_{mx} = \delta_{mz} = 43\,\mathrm{nm}$
$\delta_{px} = \delta_{pz} = 43\,\mathrm{nm}$	

With the discretized time index j, the time-dependent polarization and magnetization at each layer are denoted by $P^{(i)}(j)$ and $M^{(i)}(j)$. The time-dependent external sinusoidal electric field and magnetic field applied along the z direction are given by $E^{(i)}(j) = E_0 \sin(2\pi f^E_n j \Delta t)$ and $H^{(i)}(j) = H_0 \sin(2\pi f^M_n j \Delta t)$, respectively. E_0, H_0 and f^E_n, f^M_n are the amplitude and frequency, respectively. By taking the forward difference in time for the left-hand side of equations (23) and (24), we can obtain the polarization and magnetization of each layer at each time. The average values at each discretized time point are the summations of each layer divided by the total layer number.

3. Results and discussions

We took $BaTiO_3$–$CoFe_2O_4$ as an example on a $SrTiO_3$ substrate system. The parameters taken from [20, 36] are listed in table 1. Because of the limited experimental data, D^M_{11}, D^M_{44} and critical thicknesses h^p_ρ and h^m_ρ were given with considerable values. The values of the extrapolation lengths are usually about 5–45 nm for $BaTiO_3$; here, 43 nm is used for the two phases, which may add some discrepancy especially when the volume fraction of portion is very small. The total length of the sample l was taken as 100 nm.

Firstly, we give the para–ferro phase transition temperatures under different thicknesses of the film (figure 2). Since the critical temperature of $CoFe_2O_4$ is usually higher than that of the $BaTiO_3$, we set $P = 0$, $m = 1$ in figure 2(*a*) and $P = 0$, $m = 0$ in figure 2(*b*) as initial states to derive the para–ferro phase transition temperatures. The results show a significant decrease in phase transition temperatures for both parts with the increase in thickness. It is well known that the critical phase transition temperatures are very sensitive to the stress which is induced by the misfit stress induced from the film/substrate or other stress/strain projects [36, 37]. The misfit stress from the film/substrate is highly dependent on lattice parameters and the volume fractions of each part. Because of the dislocations during the growth of films, the misfit stress is also highly dependent on the film thickness because of the relaxation of the stress with the increase in the film thickness. In the 1–3 type $BaTiO_3$–$CoFe_2O_4$ structure, the misfit stress is very large, especially in the interface of the two phases along the vertical direction. So the properties of such highly strained structure can be very different from those of the bulk counterparts. The large misfit stress is also the main cause of the increase in the phase transition temperature.

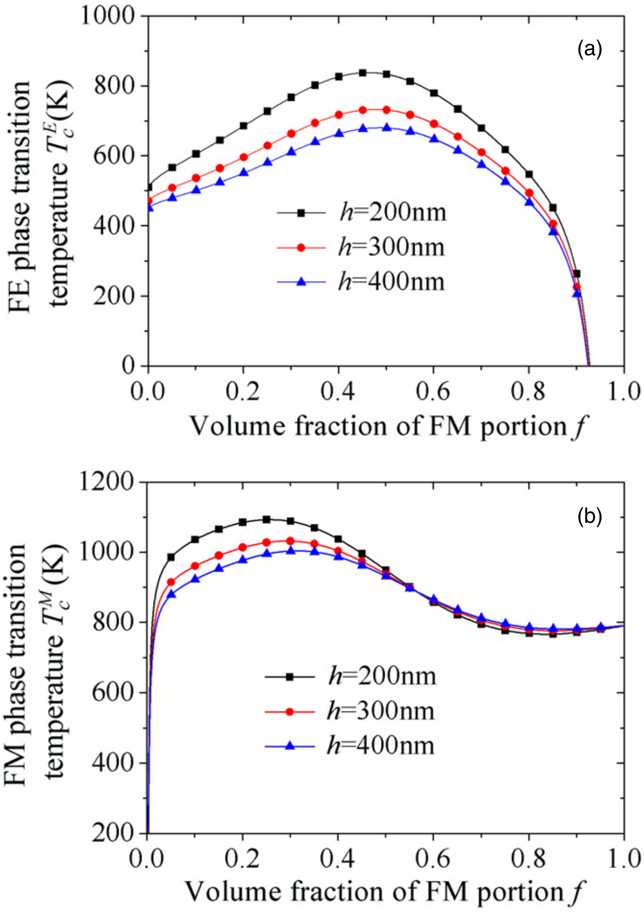

Figure 2. Para–ferro phase transition temperature. (*a*) $BaTiO_3$, $P = 0$ and $m = 1$; (*b*) $CoFe_2O_4$, $m = 0$ and $P = 0$.

To investigate the spontaneous polarization effect on the phase transition temperature of the FM portion and the spontaneous magnetization effect on the phase transition temperature of the FE portion, we contrast phase transition temperatures between the initial value of $P = 0$, $m = 1$ and the value of $P = 0$, $m = 0$ for $BaTiO_3$ as shown in figure 3(*a*) and the initial value of $m = 0$, $P = 0$ and the value of $m = 0$, $P = 0.25$ for $CoFe_2O_4$ as shown

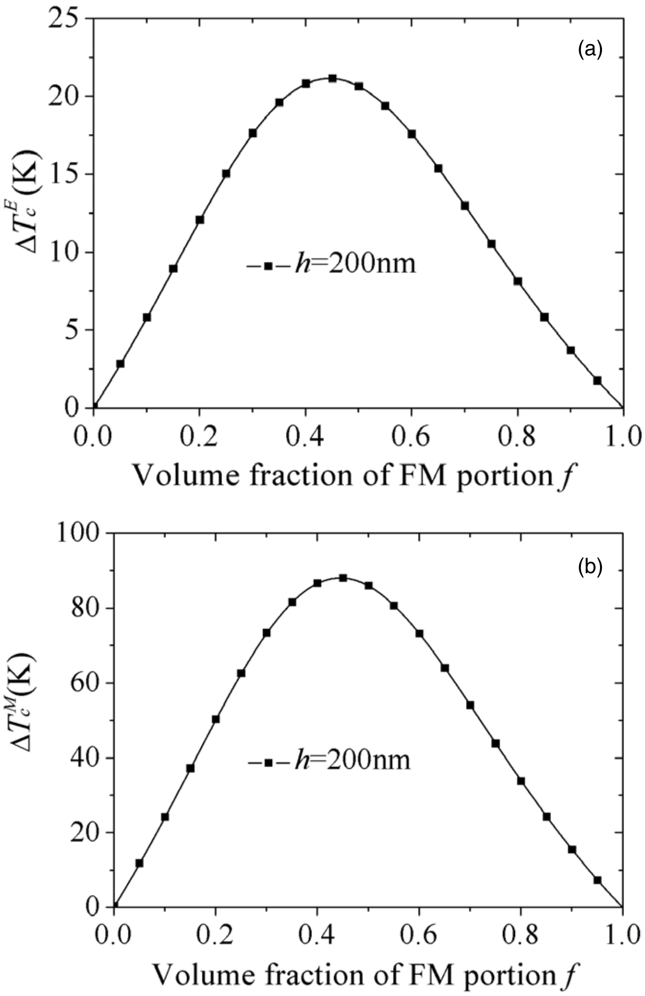

Figure 3. Difference of phase transition temperature (*a*) between the initial value of $P = 0$, $m = 1$ and the value of $P = 0$ and $m = 0$ for $BaTiO_3$; (*b*) between the initial value of $m = 0$, $P = 0$ and the value of $m = 0$, $P = 0.25$ for $CoFe_2O_4$.

in figure 3(*b*). As anticipated, the spontaneous polarization induced phase transition temperature of the FM portion is large, while the spontaneous magnetization induced phase transition temperature of the FE portion is small. As shown in the analytic expressions of the phase transition temperatures (equations (18) and (19)), the magnetostriction and electrostriction are very important factors for the direct coupling effect. Although the magnetostriction of $CoFe_2O_4$ is large among the ferries, it is still small compared with the electrostriction of $BaTiO_3$. The induced magnetostrictive strain is much smaller than the electrostrictive strain and the misfit strain induced by the lattice mismatch. This is why the ME effect is usually not very significant. Although the decrease in FE phase transition temperature between $m = 0$ and $m = 1$ is small compared with its bulk Curie temperature, it is very helpful to design agile devices and microwave devices [38].

As illustrated above, the spontaneous polarization and magnetization is also highly thickness and volume fraction dependent (figure 4). The sharp decrease in polarization and increase in magnetization are mainly caused by the surface effect. In fact, just as the change in temperature, the polarization has little change with the increase in the magnetization value. But the change in polarization can still give a visible increase in magnetization as shown in the inset of figure 4(*b*). We know that the ME effect is small in the 2–2 type because of the clamp of the substrate, and the 1–3 type structure had a higher ME effect. Although it is a better structure, the clamp effect is still large due to the large misfit strain. A better solution may be to find appropriate materials with comparable lattice parameters, most importantly, with comparable magnetostriction and electrostriction.

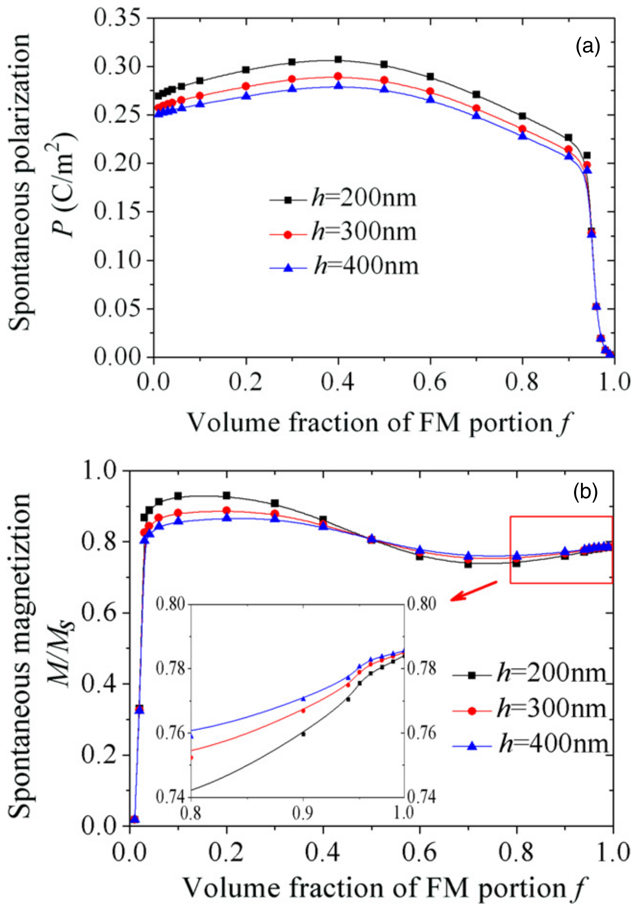

Figure 4. Spontaneous polarization (*a*) and magnetization (*b*) versus the volume fraction under different film thicknesses (inset is the zoom in the frame for easy view).

To give a clear stress field of the system, we gave the average total stresses (figure 5). Both the substrate induced transverse total strain (ε_{11}^0) and the resulting vertical strains considering the misfit of the two parts ($\varepsilon_{33}^{\mathrm{p}}$ and $\varepsilon_{33}^{\mathrm{m}}$) have a significant thickness effect and volume fraction dependence. In the $BaTiO_3$ portion, an in-plane constraint and/or an out-of-plane tension will increase the electric polarization in the vertical direction, while in the $CoFe_2O_4$ portion, with a negative magnetostrictive coefficient, an out-of-plane constraint will help the magnetic polarization in the vertical direction. The 1–3 type of this composite is helpful for both phase transitions in the vertical direction. But because of the negative average in-plane stress ε_{11}^0, the value of average vertical strain in the FM part $\varepsilon_{33}^{\mathrm{m}}$ is negative when f is only less than about 0.4 and turns out to be positive as the

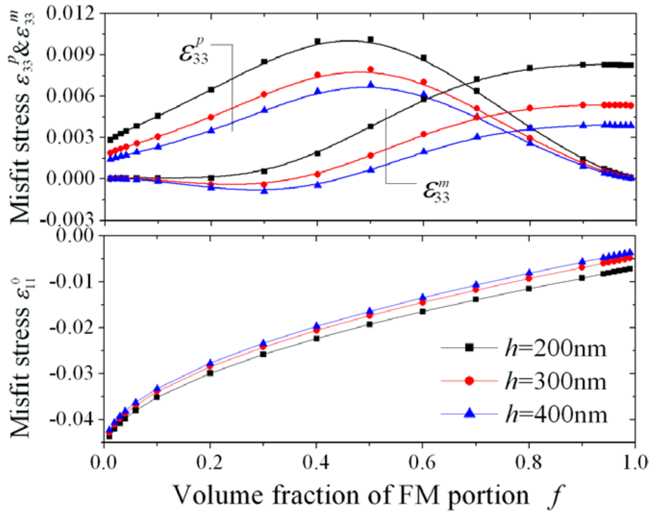

Figure 5. Average in-plane total strain ε_{11}^{0}, vertical strains in the FE portion $\varepsilon_{33}^{\mathrm{p}}$ and vertical strain in the FM portion $\varepsilon_{33}^{\mathrm{m}}$ under different film thicknesses.

volume fraction of the FM part increases, which hampers the FM phase polarization. Besides, the stress induced by the spontaneous polarization will weaken the compression in the vertical direction and hamper the magnetization phase transition and vise versa.

Finally, we simulated hysteresis loops under different external fields mathematically. Many experiments have shown that multiferroic composites have different responses to different external fields [39, 40] (such as dc/ac single field, double field, pulse field). Because of the effect of the external stress induced from the substrate and the interface stress between the two portions, the P and M are enhanced as expected. Of our interest is the basic function of multiferroic materials, that is, the magnetization simulated by the external electric field and the polarization by the external magnetic field. We plot the M–E and P–H loops as shown in figure 6. Butterfly loops exist under ac external fields with big enough amplitudes. Because of the second order relationship of stress, there is no reversion of order parameters, that is, the single-cross-field induced polarization or magnetization are always in the same direction with the value changed as a butterfly loop.

4. Conclusions

We investigated the effect of thickness on the stress state in a composite of BaTiO$_3$–CoFe$_2$O$_4$ film on a SrTiO$_3$ substrate system using Landau phenomenological theory. The misfit stress induced by the lattice mismatch from the FE/FM and the film/substrate interfaces can significantly affect the properties of each component in the multiferroic composite structure, but the direct elastic interaction is small because of the small magnetostriction and the clamping effect of the mismatch strain. Well-matched heterostructures made up of materials with comparable magnetostriction and electrostriction are suggested for reaching a large ME effect.

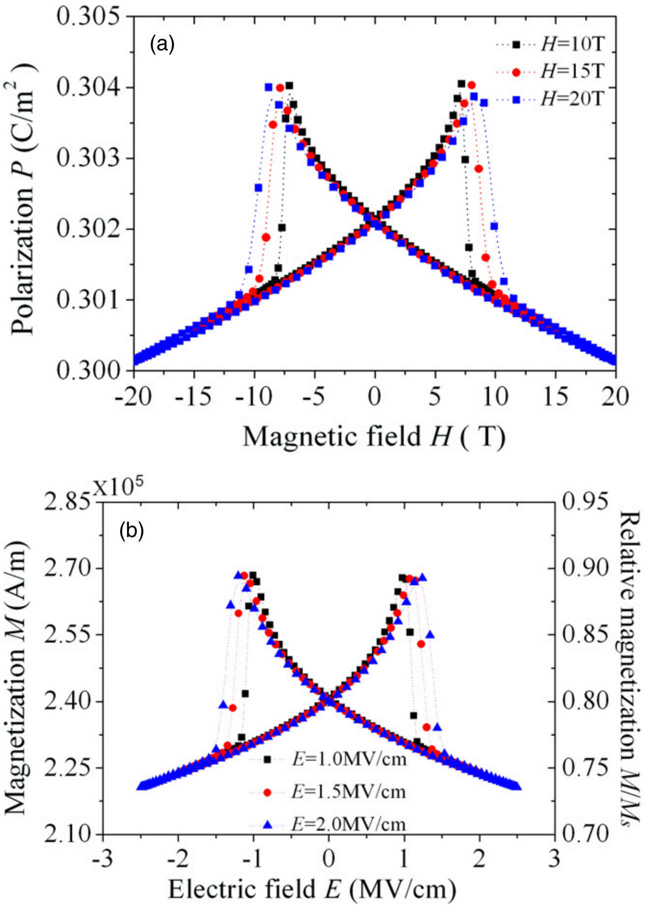

Figure 6. (*a*) Butterfly loops of spontaneous polarization of BaTiO$_3$ on the external magnetic fields with different amplitudes; (*b*) butterfly loops of magnetization of CoFe$_2$O$_4$ on the external electric fields with different amplitudes.

Acknowledgments

This project was supported by the National Science Foundation of China (Nos 10172030, 10732100 and 10572155), the Ministry of Education PRC Special Scientific Research Fund for Doctor Subjects in Colleges and Universities (20060558070) and the Science Foundation of Guangzhou Province (2005A10602002).

References

[1] Ramesh R and Spaldin N A 2007 *Nature Mater.* **6** 21
[2] Cheong S W and Mostovoy M 2007 *Nature Mater.* **6** 13
[3] Nan C W, Bichurin M I, Dong S X, Viehland D and Srinivasan G 2008 *J. Appl. Phys.* **103** 031101
[4] Lee S *et al* 2008 *Nature* **451** 805
[5] Prellier W, Singh M P and Murugavel P 2005 *J. Phys.: Condens. Matter* **17** R803
[6] Singh M P, Prellier W, Mechin L and Raveau B 2006 *Appl. Phys. Lett.* **88** 012903
[7] Murugavel P, Singh M P, Prellier W, Mercey B, Simon Ch and Raveau B 2005 *J. Appl. Phys.* **97** 103914
[8] Liu M, Li X, Imrane H, Chen Y, Goodrich T, Cai Z, Ziemer K S, Huang J Y and Sun N X 2007 *Appl. Phys. Lett.* **90** 152501
[9] Liu G, Nan C W and Sun J 2006 *Acta Mater.* **54** 917

[10] Artemev A, Slutsker J and Roytburd A L 2005 *Acta Mater.* **53** 3425

[11] Erenstein W, Mathur N D and Scott J F 2006 *Nature* **442** 17

[12] Zheng H, Straub F, Zhan Q, Yang P L, Hsieh W K, Zavaliche F, Chu Y H, Dahmen U and Ramesh R 2006 *Adv. Mater.* **18** 2747

[13] Zavaliche F, Zhao T, Zheng H, Straub F, Cruz M P, Yang P L, Hao D and Ramesh R 2007 *Nano Lett.* **7** 1586

[14] Zheng H *et al* 2004 *Science* **303** 661

[15] MacManus-Driscoll J L, Zerrer P, Wang H, Yang H, Yoon J, Fouchet A, Yu R, Blamire M G and Jia Q 2008 *Nature Mater.* **7** 314

[16] Lu XY, Wang B, Zheng Y and Ryba E 2007 *Appl. Phys. Lett.* **90** 133124

[17] Deng C Y, Zhang Y, Ma J, Lin Y H and Nan C W 2008 *Acta Mater.* **56** 405

[18] Slutsker J, Levin I, Li J H, Artemev A and Roytburd A L 2006 *Phys. Rev.* B **73** 184127

[19] Wu T, Zurbuchen M A, Saha S, Wang R V, Streiffer S K and Mitchell J F 2006 *Phys. Rev.* B **73** 134416

[20] Nan C W, Liu G, Lin Y H and Chen H D 2005 *Phys. Rev. Lett.* **94** 197203

[21] Liu G, Nan C W, Xu Z K and Chen H D 2005 *J. Phys. D: Appl. Phys.* **38** 2321

[22] Slutsker J, Tan Z P, Roytburd A L and Levin I 2007 *J. Mater. Res.* **22** 2087

[23] Chambers S A, Farrow R F C, Maat S, Toney M F, Folks L, Catalano J G, Trainor T P and Brown G E 2002 *J. Magn. Magn. Mater.* **246** 124

[24] Brown G, Novotny M A and Rikvold P A 2001 *Phys. Rev.* B **64** 134422

[25] Porta M, Castán T, Planes A and Saxena A 2005 *Phys. Rev.* B **72** 054111

[26] Woo C H and Zheng Y 2008 *Appl. Phys.* A **91** 59

[27] Li Y L, Hu S Y, Liu Z K and Chen L Q 2002 *Acta Mater.* **50** 395

[28] Wang B and Woo C H 2008 *J. Appl. Phys.* **103** 12410

[29] Zhong L, Wang Y G, Zhang P L and Qu B D 1994 *Phys. Rev.* B **50** 698

[30] Cottam M G, Tilley D R and Zeks B 1984 *J. Phys. C: Solid State Phys.* **17** 1793

[31] Zhang J X, Li Y L, Schlom D G, Chen L Q, Zavaliche F, Ramesh R and Jia Q X 2007 *Appl. Phys. Lett.* **90** 052909

[32] Alpay S P and Roytburd A L 1998 *J. Appl. Phys.* **83** 4714

[33] Lu X Y, Wang B, Zheng Y and Ryba E 2007 *J. Phys. D: Appl. Phys.* **40** 1614

[34] Wang B and Woo C H 2005 *J. Appl. Phys.* **97** 084109

[35] Lo V C 2003 *J. Appl. Phys.* **94** 3353

[36] Pertsev N A, Zembilgotov A G and Tagantsev A K 1998 *Phys. Rev. Lett.* **80** 1988

[37] Zheng Y, Woo C H and Wang B 2007 *J. Appl. Phys.* **101** 116103

[38] Lu X Y, Wang B, Zheng Y, Liu Y L and Li C L 2008 *J. Phys. D: Appl. Phys.* **41** 095004

[39] Yin X M, Zhang N and Bao J C 2007 *Phys. Lett.* A **361** 434

[40] Bueno-Baques D, Grossinger R, Schonhart M, Doung G V, Sato R, Corral-Flores V and Matutes-Aquino J 2006 *J. Appl. Phys.* **99** 08D908